Supercapacitors based on nitrogen-enriched crumpled graphene with a high volumetric capacitance and high-mass-loading per area of the electrode

YU Qiong, WANG Yong-zhi, MENG Meng, SHEN Shu-ling, TANG Zhi-hong*, YANG Jun-he

(*School of Materials Science and Engineering*, *University of Shanghai for Science and Technology*, *Shanghai* 200093, *China*)

Abstract: The low volumetric capacity and sluggish diffusion of ions at high mass loadings of active materials per area limit any improvement of the energy and power densities of supercapacitors. A mixture of graphene oxide (GO) and urea in water was treated by an ultrasonic atomizer to form aerosol droplets, which were dried to obtain crumpled GO/urea particles. Crumpled graphene with a nitrogen content of 11.38% was obtained by the thermal shocking of these particles at 600 °C for 50 s. A volumetric capacitance of 384.0 F cm^{-3} was achieved when the crumpled graphene was used as supercapacitor electrodes. Even at a high current density (10 A g^{-1}) and a high loading (74.3 mg/cm^2 electrode), the specific capacitance retention still remained high. It is proposed that N-doping in the forms of pyrrole, imide, lactam and other types of pyridine-like nitrogen, and high surface area of the sample were key factors in improving the capacitance. The crumpled structure provided high mass transfer and high accessibility of ions to the active surface.

Key words: Crumpled graphene; Nitrogen; Heat shock; Supercapacitor

1 Introduction

The supercapacitors have attracted much attention owing to their high power density. Considerable efforts have been made to improve the gravimetric capacity of supercapacitors by optimizing pore structures or introducing pseudocapacitive effects[1–5]. For portable electronic and electric automobiles, however, volumetric capacity and mass loading per area are more important[6–8]. Up to now, the highest volumetric capacity is obtained from a RuO_2 based capacitor, which can reach 1 000 to 1 500 F cm^{-3} with excellent cycling stability, but the loading mass per area is low[9]. Additionally, the price of RuO_2 is too high to commercialize. Thus, various electrode materials with pseudocapacitive properties, such as MnO_2, NiO and polyaniline, have been exploited[10–13]. These materials deliver high volumetric capacity but still suffer from poor cycling performance. To overcome the barriers mentioned above, carbon-based materials are utilized, and particular attention is given to metal carbides and graphene. Graphene is more cost-effective compared with metal carbides.

Graphene-based electrodes for supercapacitors are widely used due to the unique electronic property, low density, and ultrahigh surface area[14, 15]. It has a theoretical double-layer capacitance of about 550 F g^{-1}. However, in practice, graphene has to be packed tightly to achieve high volumetric capacity with the sacrifice of surface area utilization. Doping with heteroatoms is a good option to compensate for this deficiency and improve its electrochemical performance[16, 17]. The pseudocapacitive mechanism induced by the heteroatoms endows nitrogen or oxygen doped graphene with high capacitance and excellent stability, due to the nitrogen (pyrrolic-N, pyridone-N, and pyridinic-N) and oxygen-containing functional groups[18–20]. Based on this theory, many excellent results have been achieved. Graphite with a density of 1.58 g cm^{-3} (the surface oxygen content about 4 at.%) was prepared by evaporation-induced drying of a graphene hydrogel, whose volumetric capacitance could be up to 376 F cm^{-3}[21]. Fan et al. synthesized a N-doped graphene/porous carbon (SGC) hybrid by one-step pyrolysis of the mixture of graphene oxide/polyaniline hybrid and KOH activation. SGC

Received date: 2020-11-18; **Revised date:** 2021-04-10

Corresponding author: TANG Zhi-hong, Associate Professor. E-mail: zhtang@usst.edu.cn

Author introduction: YU Qiong. E-mail: 2388860345@qq.com

Supplementary data associated with this article can be found in the online version.

exhibited a volumetric capacitance of 212 F cm^{-3} in an aqueous electrolyte[22]. Besides, the volumetric capacitance can also be increased by using graphene-based composites. A composite of graphene with polyaniline was fabricated by polymerization of aniline monomer in a graphene monolith, whose volumetric capacitance reached more than 570 F cm^{-3}[23]. The N-doped holey graphene/PANI delivered a ultrahigh volumetric capacitance (1 058 F cm^{-3} at 0.5 A g^{-1}), and the capacitance retention was 81.5% after 5 000 cycles[24]. However, the increased diffusion resistance made the capacitance decay seriously when the loading of the active component per area increased. In practice, increasing the loading of the active material per area while remaining high capacitive performance, is of crucial importance. The high mass loading per area ensures the high energy density. This will also contribute to the development of high-power, miniaturized, lightweight and low-cost supercapacitors[25]. Huang et al. used a 3D crumpled graphene as an active material of the supercapacitor electrode, the high retention rate was obtained when the loading amount increased from 2 to 16 mg per area of the electrode[26]. Unfortunately, the volumetric capacity of the 3D crumpled graphene ball was only about 60 F cm^{-3}. Although much progress has been achieved, designing and fabricating new kinds of graphene-based materials with high volumetric capacity and high mass loading per area simultaneously are still a significant challenge.

Herein, we present a simple and green method to prepare nitrogen-enriched crumpled graphenes (NCGs). The unique crumpled structure provided the fast diffusion kinetics of ions and the large mass loading as per electrode area. The abundant nitrogen improved the capacitive performance of the materials. The volumetric capacitance of the optimized NCG was 384 F cm^{-3}, and the specific capacitance retention was 76.3% when the current density was increased to 10 A g^{-1}. More importantly, even when the mass-loading increased from 1.71 to 21.00 mg per area, the specific capacitance still retained 83.6%.

2 Materials and methods

2.1 Preparation of NCG Experimental

The preparation of NCGs is schematically illustrated in Fig. 1a. Graphene oxide (GO) and urea were mixed, and the mixture formed aerosol droplets under the action of an ultrasonic atomizer (1.7 MHz). Then the aerosol droplets flew through a preheated tube furnace pushed by the pressure differentials. A Teflon filter was placed at the end of the quartz tube to collect the crumpled graphene oxide/urea nanoparticles (CGU). CGU was dried and then heat shocked at 600 °C for 50 s, 90 s, 180 s and 600 s to obtain the samples named as NCG-50, NCG-90, NCG-180 and NCG-600, respectively.

2.2 Characterization

Scanning electron microscopy (SEM) (FEI Quanta FEG) and transmission electron microscopy (TEM) (Tecnai G2 F30) were used to observe the microscopic morphology and microstructure of the samples. XPS was used to characterize the chemical bonds and functional groups of the samples. Pore structure of the sample was tested on the Micromeritics ASAP-2020 at 77 K, and the specific surface area was calculated using the Brunner-Emmet-Teller (BET) method. Using Bruker's D8-Advanced diffractometer, X-ray diffraction (XRD) patterns were detected using Cu $K\alpha$ radiation (λ = 0.154 18 nm). Functional groups of the samples were tested by Fourier transform infrared spectroscopy (FTIR) on a Perkin Elmer's Spectrum 100 spectrometer, which was equipped with an attenuated total reflectance (ATR) sample holder.

2.3 Electrochemical tests

Electrochemical tests were conducted using a three-electrode system, the electrochemical workstation was CHI650D (Chenhua Instruments, China), and the electrolyte solution was 6 mol L^{-1} KOH. The reference electrode was Ag/AgCl, the counter electrode was Pt, and the working electrode was made of NCG-90. The specific preparation method of the working electrode was as follows. As-prepared samples were mixed with polytetrafluoroethylene (PTFE) with a

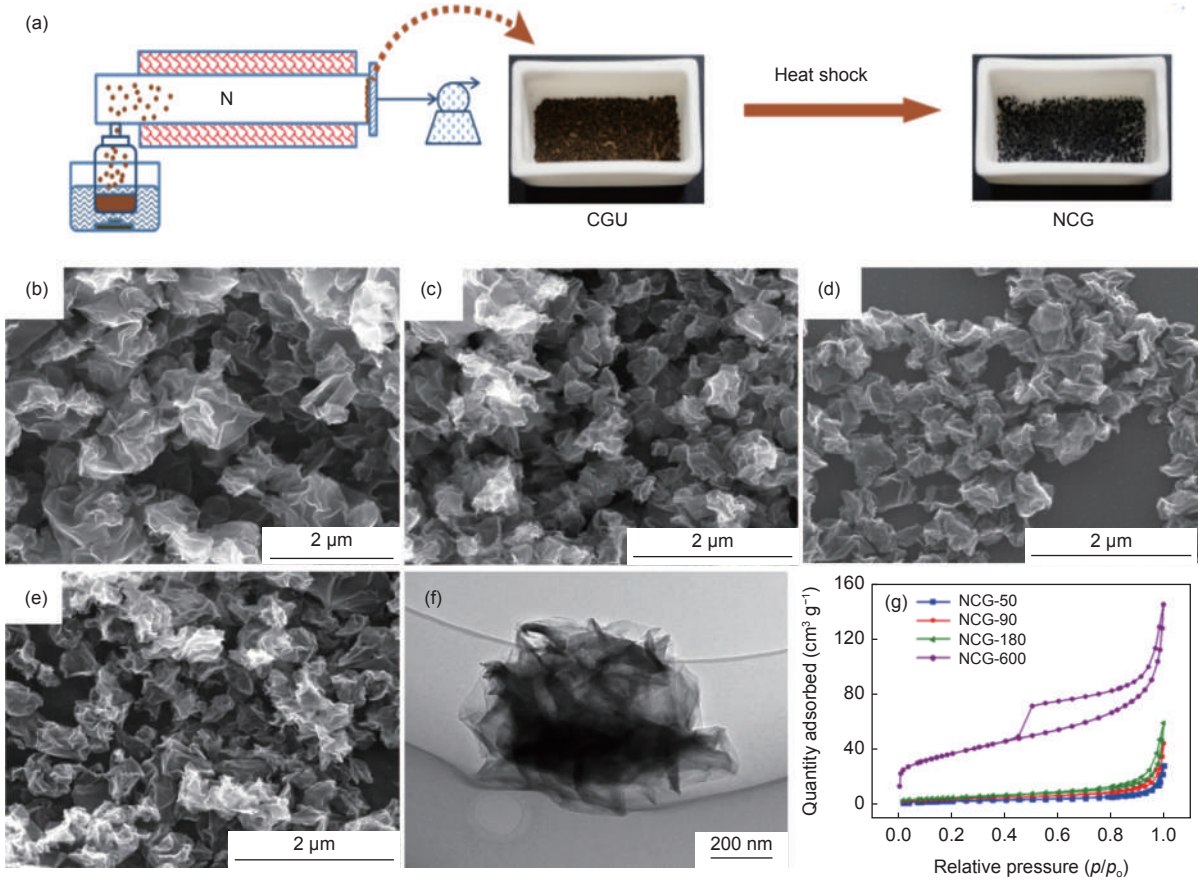

Fig. 1　(a) Schematic illustration of the preparation of NCG. SEM images of (b) NCG-50, (c) NCG-90, (d) NCG-180 and (e) NCG-600. (f) TEM image of NCG-90. (g) N_2 adsorption/desorption isotherms of NCGs. .

mass ratio of 9∶1. The mixture was stirred into a slurry after a small amount of deionized water was added. A certain amount of the slurry was rolled into a uniform film, then it was pressed into the electrode with a diameter of 6 mm. In the end, the electrode was dried a vacuum oven at 100 °C for 24 h. Cyclic voltammetry (CV) at different scan rates of the samples was carried out in a voltage window of 0--1.0 V. Galvanostatic charge-discharge (GCD) curves at different current densities and electrochemical impedance spectra (EIS) were measured. For the device of the supercapacitor, as-prepared electrodes were assembled into a coin type of capacitors, and they were used to light the diodes.

3　Results and discussion

Transmission electron microscopy (TEM) was used to observe the morphology and microstructure of as-prepared samples: NCG-50, NCG-90, NCG-180, NCG-600. As shown in Fig. 1b-e, all the samples show a crumpled structure, even though they suffered a heat shock at 600 °C for 50-600 s. Compared with the morphology of CGU shown in Fig. S1, the ridges of the NCGs became sharper, indicating the urea was decomposed after the heat shock. The TEM image of NCG-90 further revealed the crumpled structure (Fig. 1f). The TEM image of NCG-90 was dark in the center, indicating that urea was not decomposed completely.

Nitrogen adsorption was used to characterize the pore structure of NCGs at 77 K. As shown in Fig. 1g, the nitrogen adsorption amounts of NCG-50, NCG-90, and NCG-180 increased slightly with the thermal shock time, whose Brunner Emmet Teller (BET) specific surface area (SSA) were 11.1, 15.5 and 20.1 $m^2\ g^{-1}$, respectively. As the heat shock time increased to 600 s, the nitrogen adsorption amount increased significantly, and SSA reached 130.0 $m^2\ g^{-1}$,

whose adsorption/desorption isotherm had a visible hysteresis loop, suggesting the coexistence of micropores and mesopores[27]. Furthermore, density functional theory (DFT) model was used to calculate the pore size distribution (Fig. S2), which suggested the pores of NCG-50, NCG-90, and NCG-180 were mainly larger than 10 nm. On the contrary, the pore structure of NCG-600 was different. A large number of micropores (~1.2 nm) appeared, and its pore volume increased to 0.17 $cm^3\ g^{-1}$. A possible reason was that when the CGU was heat-treated at 600 °C, the urea was decomposed into nitrogen compounds such as ammonia, cyanuric acid, H_2O and CO_2. In the meantime, nitrogen compounds could also react with GO. When the heating time was short (less than 90 s in the experiment), the nitrogen compounds didn't have enough time to decompose, and they would deposit on the surface of crumpled graphene, which was consistent with the low SSA and the dark TEM image of NCG-90. Prolonging the heating time to 600 s, the nitrogen compounds deposited on the surface area of graphene decomposed completely, only the functional groups reacted with GO remained, so more pores appeared.

X-ray diffraction (XRD) patterns and FTIR spectra (Fig. 2a, b) were used to explore further the chemical properties of the derivatives of GO and urea. There were two sharp diffraction peaks at 19.8° and 29.8° for NCG-50, which were attributed to the (111) and (202) crystal plane of cyanuric acid. Another characteristic diffraction peak of cyanuric acid at 26.3° (−211) seemed broad, and it was believed that the peak was overlapped with the broad peak at 25.8° (002) of reduced GO. For NCG-90, the intensities of the two characteristic diffraction peaks of cyanuric acid became much weak. Further prolonging the heat shock time, for NCG-180 and NCG-600, the characteristic diffraction peaks of cyanuric acid disappeared.

Meanwhile, the diffraction peak (002) of reduced GO became strong, indicating the decomposition of urea and reduction of crumpled GO gradually[28, 29]. FTIR spectra shown in Fig. 2b agreed well with the results from the analysis of XRD. Peaks at about 1 000-1 350 cm^{-1} were ascribed to C—O stretching vibration and the aromatic C—N heterocyclic, respectively. The peaks at ~755 cm^{-1} and ~1 700 cm^{-1} of NCG-50 and NCG-90 were ascribed to the triazine units and the carbonyl groups, respectively, further proving the existence of triazine derivatives[30–32]. Additionally, another typical peak at ~1 570 cm^{-1} was ascribed to the aromatic C=C stretching of graphene sheets[33–35].

The chemical bonding of the as-prepared samples was further detected by X-ray photoelectron spectroscopy (XPS). As the pyrolysis time increased, the nitrogen content in the sample decreased, and it was as high as 11.38% when the shock time was the 50 s (Table S1). Scanning transmission electron microscopy (STEM) of NCG-90 suggested the presence of C, N and O atoms, which were homogeneously distributed in the crumpled graphene framework despite the high nitrogen content (Fig. S3). According to the C 1s spectra (Fig. S4), there were five kinds of carbon species, including 284.8 eV for C—C, 285.6 eV

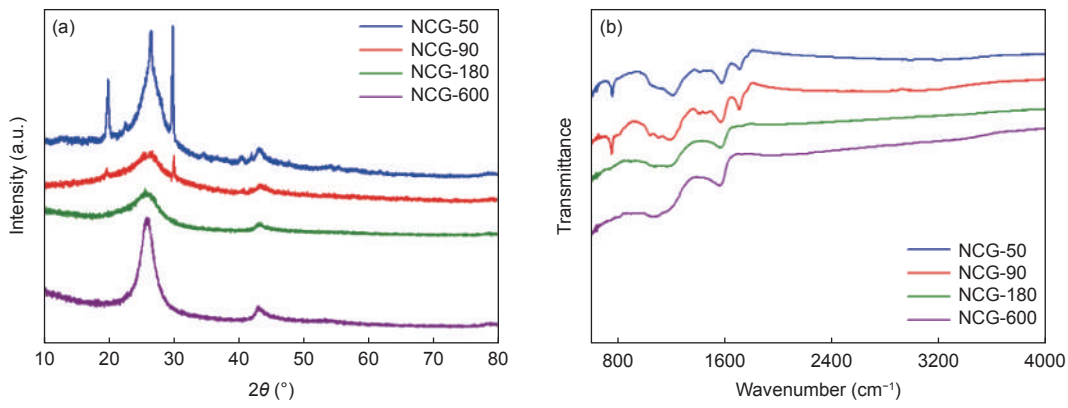

Fig. 2 (a) XRD patterns and (b) FTIR spectra of NCGs.

for C—N, 286.5 eV for C—O, 287.5 eV for C=O and 288.7 eV for O—C=O, indicating the existence of nitrogen functional groups. The N 1s spectra (Fig. 3) were well fitted into three N species, 398.7 eV for N1 (pyridine), 400.0 eV for N2 (pyrrole, imide, lactam, or other forms of pyridine-like nitrogen), and 401.0 eV for N3 (quaternary nitrogen). The molar ratios of different types N were listed in Table S1. In NCG-50 and NCG-90, the primary nitrogen was N2, which resulted from triazine derivatives and the nitrogen functional groups of the graphene. In NCG-180 and NCG-600, N2 began to decrease, indicating the decomposition of triazine derivatives.

Based on the above analysis, the chemical reaction mechanism of GO and urea was depicted in Fig. 4. At the first step, urea decomposed to cyanic acid, ammonia, carbon dioxide, and water, and a small amount of NH_3 reacted with GO simultaneously as in the case of NCG-50. As reported, cyanic acid had two isomers (1,3,5-triazinane-2,4,6-trione and 1,3,5-triazin-2,4,6-triol)[36]. When the heat shock time increased, 1,3,5-triazin-2,4,6-triol further reacted with NH_3, after which ammelide, ammeline, and melamine were formed, and the amount of cyanic acid decreased at the same time. With prolonging the heat shock time further, ammelide, ammeline, melamine, and NH_3 reacted with the functional groups of GO to form nitrogen-enriched crumpled graphene as in the case of NCG-90, which was proved by the analysis of XRD, XPS and nitrogen adsorption. Further increasing the heat treatment time, N2 species (pyrrole, imide, lactam, or other forms of pyridine-like nitrogen) were unstable at high temperatures, which were further decomposed. As the heating time increased to 600 seconds, these N2 species were almost decomposed completely, and micropores appeared.

The crumpled structure of NCGs prevented them from restacking, and therefore fast mass transfer would be achieved when they were used as active materials of supercapacitors. Furthermore, the more nitrogen functional groups especially N2 of the samples, would provide more active sites for improving the capacity. It can be predicted that the NCGs can demonstrate excellent performance as supercapacitor elec-

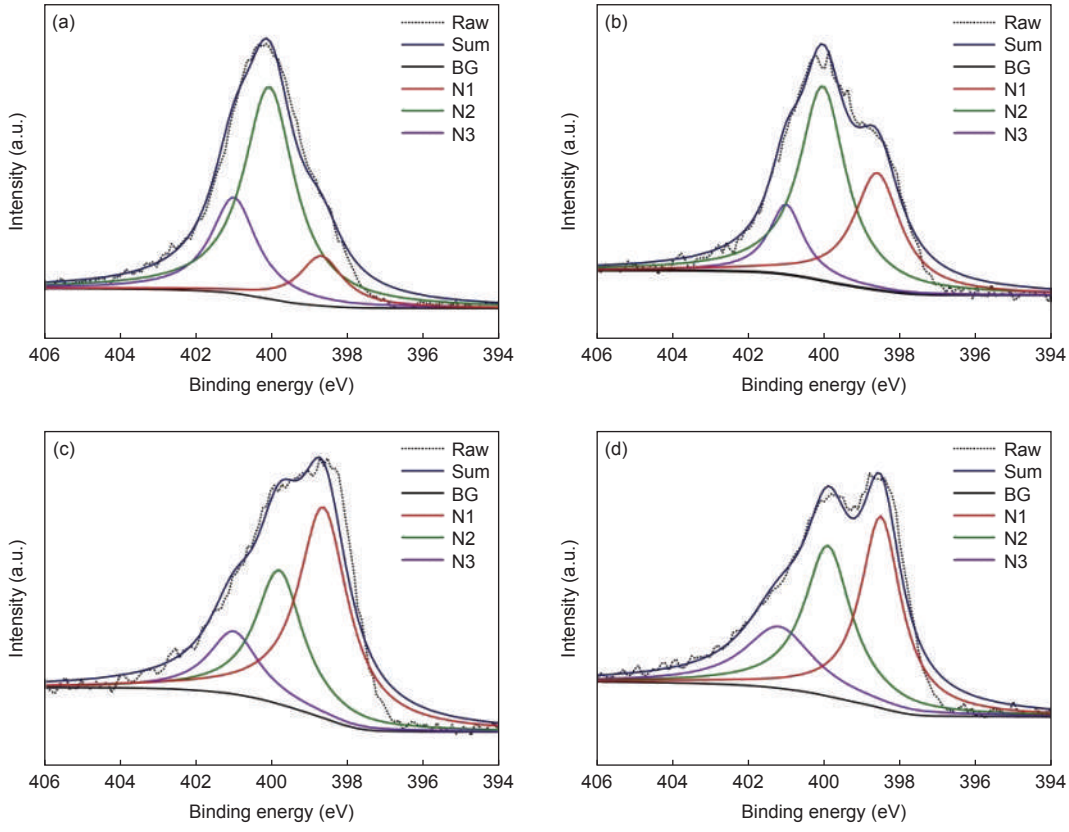

Fig. 3　N 1s spectra of the NCGs: (a) NCG -50, (b) NCG -90, (c) NCG -180 and (d) NCG -600.

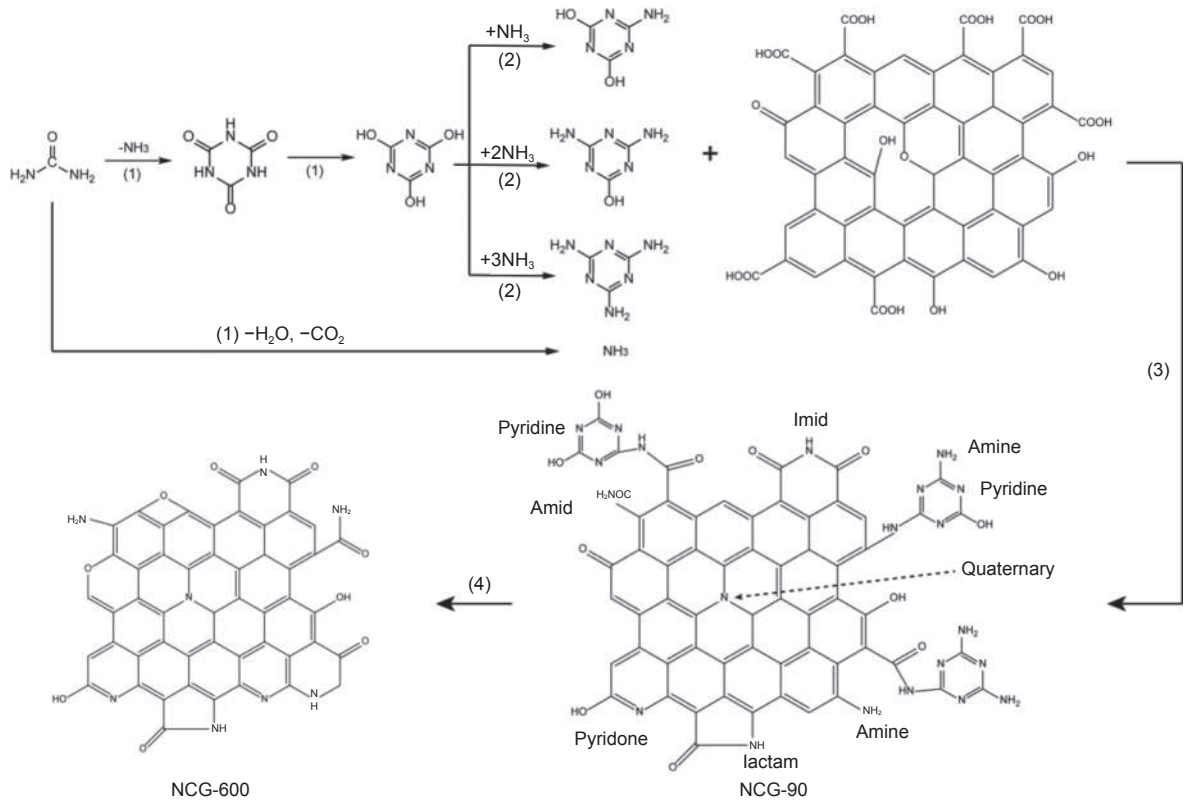

Fig. 4 The chemical reaction mechanism of GO and urea at 600 °C in the heat shock process.

trode materials. The sample was mixed with a binder (PVDF, 10%) to make electrodes. The electrochemical performance was evaluated in the three-electrode system. As shown in Fig. 5a, gravimetric capacitances of all the samples were plotted. Among them, according to the calculation of the galvanostatic discharge (GCD) curves in Fig. S5a, it was found that NCG-90 had the highest gravimetric capacitance (218.2 F g^{-1}) when the scan rate was 0.1 A g^{-1}. When it was converted to volumetric capacitance at a current density of 0.1 A g^{-1}, the volume capacitance of NCG-90 reached 384.0 F cm^{-3}, according to the calculated material density of 1.76 g cm^{-3} for NCG-90 (Fig. 5b). As far as we know, when water-based electrolytes were used, among the currently reported nonmetallic materials, the volumetric capacitance of NCG-90 was one of the highest values (Table S2). Moreover, when the current density was increased to 10 A g^{-1}, the NCG-90 still provided a capacitance of 299.6 F cm^{-3}, which was 78% of the 384.0 F cm^{-3} at 0.1 A g^{-1} (Fig. 5b). Comparatively, as shown in Fig. 5b, the other three samples showed a similar attenuation rate due to the same crumpled structure. Compared with the other samples, the high capacitance of NCG-90 could be attributed by the following three factors. First, the high content of N2 in the forms of pyrrole, imide, lactam, or other forms of pyridine-like nitrogen played an important role in improving the capacitance. Second, the high specific surface area contributed to more capacitance as compared with that to NCG-50. Third, the crumpled morphology was favorable for accessible surface for ions and fast transport of ions. Cyclic voltammetry (CV) curves of the NCGs showed a rectangular shape from 0 to −1.0 V (Fig. S6), which implied an excellent capacitive performance of NCGs. Furthermore, NCG-90 was chosen to evaluate the long-term stability. At a high current density of 5.0 A g^{-1}, NCG-90 was tested for 10 000 cycles, and it exhibited a capacitance retention of 90.1% (Fig. 5c), proving its excellent cycling stability. The outstanding cycle property may be attributed to the reversibility of the pseudocapacitive interactions, as well as the unique crumpled microstructure in graphene.

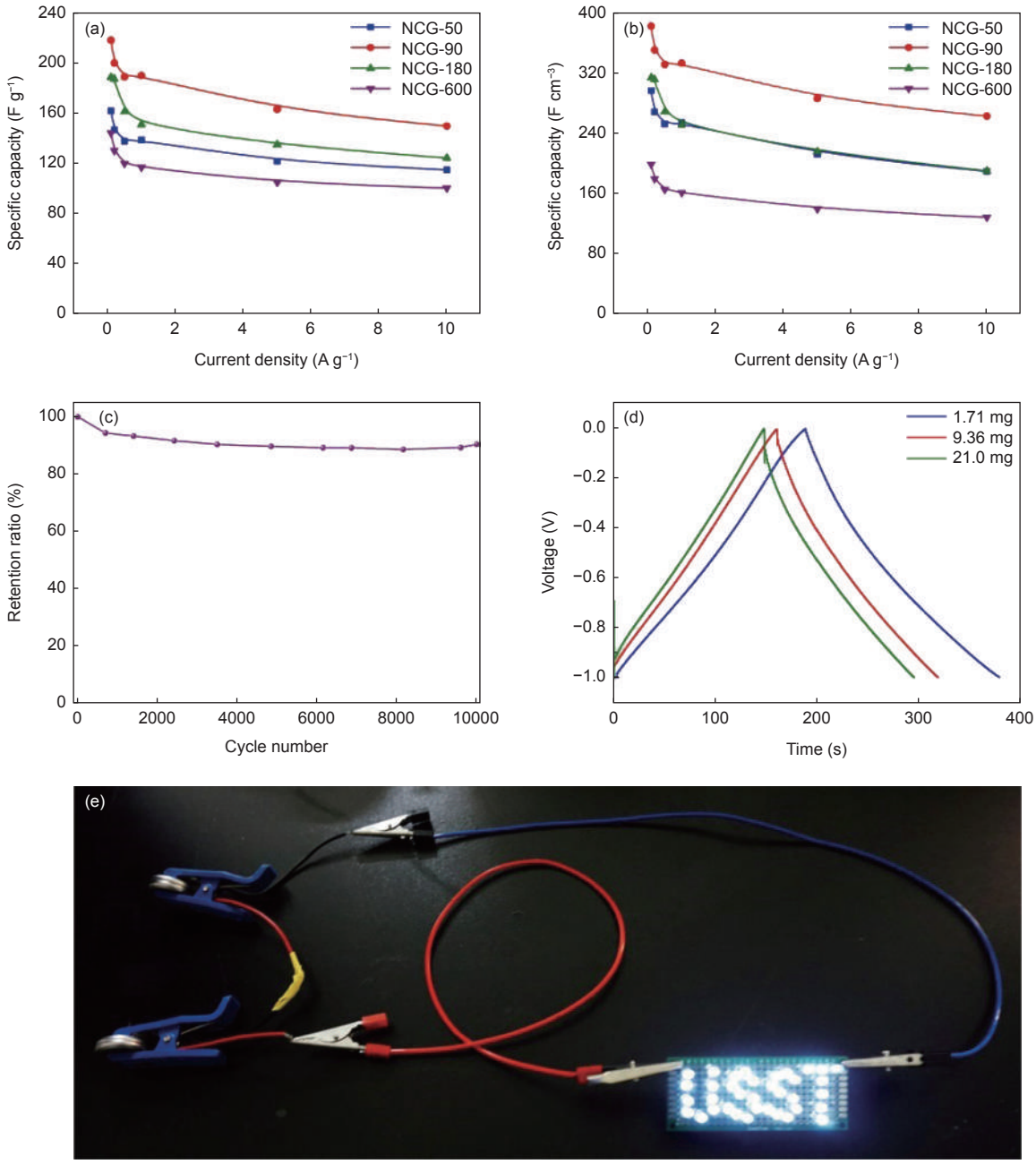

Fig. 5　(a) The gravimetric specific capacitances and (b) volumetric specific capacitances of NCGs (NCG -50, NCG-90, NCG -180 and NCG -600) with current densities ranging from 0.1 to 10 A g^{-1}. (c) Cycling stability of NCG-90 at a current density of 5.0 A g^{-1}. (d) GCD curves of the NCG-90 with different mass loadings at a current density of 1.0 A g^{-1}. (e) Digital photograph of thirty-six white light-emitting diodes "USST" powered by four supercapacitor devices connected in series.

As it is well known, ions transport perpendicular to the direction of the electrode film, the electrode thickness determines the mass loading of the active materials and the volume capacitance in the two-dimensional sheet electrodes. However, the increase in electrode thickness would result in a significant increase in the transport distance/resistance of ions and electrons in the electrodes, which in turn, lead to a severe decrease in the specific capacitance of the device at a high charge and discharge rate. In order to increase the energy density of supercapacitors in practical applications, the load level of active materials in the device should be increased. As for the NCGs, the crumpled structure facilitated the fast ion transfer in or among each particle. In the end, increasing the loading amount of the sample would not lead to the decay

of capacitance seriously. The Nyquist plots of NCGs electrodes were compared, as shown in Fig. S5c. The spectra of as-prepared samples contained two different parts: a semicircular at high-frequency region, and a line at low-frequency region. Among them, four plots had a sub-vertical slope, indicating small charge transfer resistance against the electrolyte penetration into the electrode. As the electrode materia loading increased from 1.71 to 21.00 mg of NCG-90, the specific capacitance decreased from 384 F cm^{-3} to 321 F cm^{-3} at a current density of 0.1 A g^{-1}. In other words, as the active material loading increased more than 12 times, 83.6% of the specific capacitance remained (Fig. 5d). It should be mentioned that the specific capacitance retention of NCG-90 remained 87.9% (301.5 F cm^{-3}) at the highest loading even at the current density of 1.0 A g^{-1}. As a concrete illustration of the superior electrochemical performance of the sample, devices based on NCG-90 were assembled into power supplies for the commercial electronic equipment. As many as thirty-six white light-emitting diodes (join as "USST") were powered by four tiny charged supercapacitor devices (each with the voltage of about 0.95V) (Fig. 5e). It deserved to be mentioned that the emitting-time of "USST" can sustain more than 10 min with one charge.

4 Conclusions

Nitrogen-enriched crumpled graphene samples were successfully synthesized by heat shock CGU at 600 °C for 50 s, 90 s, 180 s and 600 s. The nitrogen-enriched crumpled graphene prepared at 90 s possessed a high volumetric capacitance of 384.0 F cm^{-3} despite the ultralow SSA. Even at a high current density (10 A g^{-1}) and a high loading (21.00 mg per electrode), the specific capacitance retention could still be kept high. Our research suggested that the material with high performance can be obtained through microstructure and chemical structure design, rather than only rely on the high surface area. It was believed that this research might offer a new thought to manufacture industrial materials in energy storage and conversion systems.

Acknowledgments

This work was financially sponsored by Basic Research Program of Shanghai (19JC1410402); Scientific Research and Innovation Program of Shanghai Education Commission (2019-01-07-00-07-E00015); Shanghai Nature Science Foundation (18ZR1426300 and 18ZR1426400); and the Development Fund for Shanghai talents.

Conflicts of interest

The authors declare that they have no conflict of interest.

References

[1] Yang X D, Li Y L, Zhang P X, et al. Hierarchical hollow carbon spheres: Novel synthesis strategy, pore structure engineering and application for micro-supercapacitor[J]. Carbon, 2020, 157: 70-79.

[2] Du J, Zhang Y, Wu H X, et al. N-doped hollow mesoporous carbon spheres by improved dissolution-capture for supercapacitor[J]. Carbon, 2020, 156: 523-528.

[3] Son I S, Oh Y, Yi S H, et al. Facile fabrication of mesoporous carbon from mixed polymer precursor of PVDF and PTFE for high-power supercapacitors[J]. Carbon, 2020, 159: 283-291.

[4] Wei F, Zhang H F, He X J, et al. Synthesis of porous carbons from coal tar pitch for high-performance supercapacitors[J]. New Carbon Materials, 2019, 34(2): 132-139.

[5] Liu M J, Wei F, Yang X M, et al. Synthesis of porous graphene-like carbon materials for high-performance supercapacitors from petroleum pitch using nano-$CaCO_3$ as a template[J]. New Carbon Materials, 2018, 33(4): 316-323.

[6] Yang Z, Yang Y, Lu C X, et al. A high energy density fiber-shaped supercapacitor based on zinc-cobalt bimetallic oxide nanowire forests on carbon nanotube fibers[J]. New Carbon Materials, 2019, 34(6): 559-568.

[7] Zhang H F, Xiao D J, Li Q, et al. Porous $NiCo_2O_4$ nanowires supported on carbon cloth for flexible asymmetric supercapacitor with high energy density[J]. Journal of Energy Chemistry, 2018, 27(1): 195-202.

[8] Choudhury A, Dey B, Mahapatra S S, et al. Flexible and freestanding supercapacitor based on nanostructured poly (m-aminophenol)/carbon nanofiber hybrid mats with high energy and power densities[J]. Nanotechnology, 2018, 29: 165401.

[9] Ma H Y, Kong D B, Xu Y, et al. Disassembly-reassembly approach to RuO_2/graphene composites for ultrahigh volumetric capacitance supercapacitor[J]. Small, 2017, 13(30): 1701026.

[10] Liu Y, Jiao Y, Zhang Z L, et al. Hierarchical SnO_2 nanostructures made of intermingled ultrathin nanosheets for environmental

remediation, smart gas sensor, and supercapacitor applications[J]. ACS Applied Materials & Interfaces, 2014, 6: 2174-2184.

[11] Chen M J, Wang J Y, Tang H J, et al. Synthesis of multi-shelled MnO_2 hollow microspheres via an anion-adsorption process of hydrothermal intensification[J]. Inorganic Chemistry Frontiers, 2016, 3: 1065-1070.

[12] Xia H, Meng Y S, Yuan G L, et al. A symmetric RuO_2/RuO_2 supercapacitor operating at 1.6 V by using a neutral aqueous electrolyte[J]. Electrochemical and Solid-State Letters, 2012, 15(4): A60-A63.

[13] Kim S I, Lee J S, Ahn H J, et al. Facile route to an efficient NiO supercapacitor with a three-dimensional nanonetwork morphology[J]. ACS Applied Materials & Interfaces, 2013, 5: 1596-1603.

[14] Li J, Hao H L, Wang J J, et al. 3D Nitrogen-enriched graphene porous graphene hydrogel for high-performance supercapacitor[J]. Materials Science and Engineering, 2019, 490: 022069.

[15] Gopalsamy K, Yang Q Y, Cai S Y, et al. Wet-spun poly(ionic liquid)-graphene hybrid fibers for high performance all-solid-state flexible supercapacitors[J]. Journal of Energy Chemistry, 2019, 34: 104-110.

[16] Ji Y J, Deng Y L, Chen F, et al. Ultrathin Co_3O_4 nanosheets anchored on multi-heteroatom doped porous carbon derived from biowaste for high performance solid-state supercapacitor[J]. Carbon, 2020, 156: 359-369.

[17] Li Y, Ma W S, Sun J, et al. Electrochemical generation of Fe_3C/N-doped graphitic carbon nanozyme for efficient wound healing in vivo[J]. Carbon, 2020, 159: 149-160.

[18] Liu Y, Hao X Q, Wang L K, et al. Facile synthesis of porous carbon materials with extra high nitrogen content for supercapacitor electrodes[J]. New Journal of Chemistry, 2019, 43: 3713-3718.

[19] Xu F, Ding B C, Qiu Y Q, et al. Hollow carbon nanospheres with developed porous structure and retained N doping for facilitated electrochemical energy storage[J]. Langmuir, 2019, 35: 12889-12897.

[20] Wang J S, Qin F F, Guo Z Y, et al. Oxygen- and nitrogen-enriched honeycomb-like porous carbon from laminaria japonica with excellent supercapacitor performance in aqueous solution[J]. ACS Sustainable Chemistry & Engineering, 2019, 7: 11550-11563.

[21] Tao Y, Xie X Y, Lv W, et al. Towards ultrahigh volumetric capacitance: graphene derived highly dense but porous carbons for supercapacitors[J]. Scientific Reports, 2013, 3: 2975.

[22] Zhang Y, Wen G W, Fan S, et al. Phenolic hydroxyl functionalized partially reduced graphene oxides for symmetric supercapacitors with significantly enhanced electrochemical performance[J]. Journal of Power Sources, 2019, 435: 226799.

[23] Xu Y, Tao Y, Zheng X Y, et al. A metal - free supercapacitor electrode material with a record high volumetric capacitance over 800 F cm^{-3}[J]. Advanced materials, 2015, 27: 8082-8087.

[24] Fan Z M, Cheng Z J, Feng J Y, et al. Ultrahigh volumetric performance of a free-standing compact N-doped holey graphene/PANI slice for supercapacitors[J]. Journal of Materials Chemistry A, 2017, A: 516689.

[25] Dong Y, Zhu J Y, Li Q Q, et al. Carbon materials for high mass-loading supercapacitors: Filling the gap between new materials and practical applications[J]. Journal of Materials Chemistry A, 2020, 8: 21930-21946.

[26] Mao S, Wen Z H, Bo Z, et al. Hierarchical nanohybrids with porous CNT-networks decorated crumpled graphene balls for supercapacitors[J]. ACS Applied Materials & Interfaces, 2014, 6: 9881-9889.

[27] Ma Y X, Li X P, Shao W J, et al. Fabrication of 3D porous polyvinyl alcohol/sodium alginate/graphene oxide spherical composites for the adsorption of methylene blue[J]. Journal of nanoscience and nanotechnology, 2020, 20: 2205-2213.

[28] Mou Z G, Chen X Y, Du Y K, et al. Forming mechanism of nitrogen doped graphene prepared by thermal solid-state reaction of graphite oxide and urea[J]. Applied Surface Science, 2011, 258: 1704-1710.

[29] Sun L, Wang L, Tian C G, et al. Nitrogen-doped graphene with high nitrogen level via a one-step hydrothermal reaction of graphene oxide with urea for superior capacitive energy storage[J]. Royal Society of Chemistry Advances, 2012, 2: 4498-4506.

[30] Xiao N, Lau D, Shi W H, et al. A simple process to prepare nitrogen-modified few-layer graphene for a supercapacitor electrode[J]. Carbon, 2013, 57: 184-190.

[31] Jun Y S, Lee E Z, Wang X C, et al. From melamine - cyanuric acid supramolecular aggregates to carbon nitride hollow spheres[J]. Advanced Functional Materials, 2013, 23: 3661-3667.

[32] Lei Z B, Lu L, Zhao X S. The electrocapacitive properties of graphene oxide reduced by urea[J]. Energy & Environmental Science, 2012, 5: 6391-6399.

[33] Yuan K, Xu Y Z, Uihlein J, et al. Straightforward generation of pillared, microporous graphene frameworks for use in supercapacitors[J]. Advanced Materials, 2015, 27: 6714-6721.

[34] Sun L, Wang L, Tian C G, et al. Nitrogen-doped graphene with high nitrogen level via a one-step hydrothermal reaction of graphene oxide with urea for superior capacitive energy storage[J]. Royal Society of Chemistry Advances, 2012, 2: 4498-4506.

[35] Xu X, Zhou Y, Yuan K T, et al. Methanol electrocatalytic oxidation on Pt nanoparticles on nitrogen doped graphene prepared by the hydrothermal reaction of graphene oxide with urea[J]. Electrochim Acta, 2013, 112: 587-595.

[36] Lister M W. Some observations on cyanic acid and cyanates[J]. Canadian Journal of Chemistry, 1955, 33: 426-440.